arXiv:1511.02059v1 [physics.med-ph] 6 Nov 2015

An Intraoperative β^- Detecting Probe For Radio-Guided Surgery in Tumour Resection

Andrea Russomando*†‡, Fabio Bellini*†, Valerio Bocci†, Giacomo Chiodi†, Francesco Collamati†§, Erika De Lucia¶, Raffaella Donnarumma*, Riccardo Faccini*†, Carlo Mancini-Terracciano*†, Michela Marafini†‖, Riccardo Paramatti†, Vincenzo Patera†§‖, Luigi Recchia†, Alessio Sarti§¶, Adalberto Sciubba†§‖, Elena Solfaroli Camillocci*†, Cecilia Voena† and Silvio Morganti†

***Abstract*—The development of the β^- based radio-guided surgery aims to extend the technique to those tumours where surgery is the only possible treatment and the assessment of the resection would most profit from the low background around the lesion, as for brain tumours. Feasibility studies on meningioma, glioma, and neuroendocrine tumors already estimated the potentiality of this new treatment. To validate the technique, prototypes of the intraoperative probe required by the technique to detect β^- radiation have been developed. This paper discusses the design details of the device and the tests performed in laboratory. In such tests particular care has to be taken to reproduce the surgical field conditions. The innovative technique to produce specific phantoms and the dedicated testing protocols is described in detail.**

I. Introduction

THE main advantage of the radio-guided surgery (RGS) technique exploiting β^- radiation [1], [2], compared to the traditional RGS using γ radiation [3], is a more favourable ratio between the signal coming from the tumor and the rest of the body. Conversely to the tracers with γ emitters, pure β^- radionuclides emit electrons which penetrate only a few millimeters of tissue and produce almost no gamma radiation (the *bremsstrahlung* contribution above 100 keV being less than 0.1%) resulting in a very low background on the lesion signal.

Operating in a low background environment allows the development of a handy and compact probe which, detecting particles emitted locally, provides a clearer delineation of margins of the lesioned tissue. The RGS technique applicability can therefore be extended also to cases with large uptake of the tracer from healthy organs next to the lesion, minimizing the radiotracer activity to be administered. Low exposure of the medical team is also expected [1].

For this technique to enter in the clinical practice, relevant clinical cases need to be identified, suitable radio-tracers need to be developed for them and a detector needs to be designed and tested for this specific application.

The most relevant clinical cases are those where the RGS with γ radiation is not applicable because of the presence of uptaking organs nearby, for instance cerebral, abdominal and pediatric tumors.

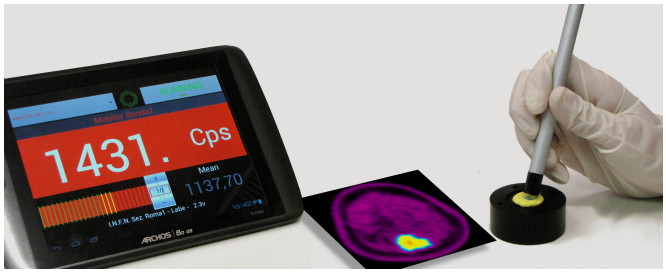

Fig. 1. Image of the intraoperative β^- probe.

Among the existing radio-tracers those that are linked to pure β^- emitters are those used in radio-methabolic treatments with ^{90}Y, such as Peptide Receptor Radionuclide Therapy [4]. Such tracers are somatostatin analogues (e.g. DOTATOC [5]) and very selective for meningioma [6] and neuroendocrine tumors (NET) [7]. Our first choice has been indeed to use meningioma as proof of principle and abdominal NETs as a first application with clinical relevance. In the case of administration of ^{90}Y-DOTATOC for meningioma, glioma and NET we have performed feasibility studies [8], [9] of which the present paper describes critical ingredients. We are finalizing the authorizations for the clinical tests. Nonetheless, to extend this technique beyond NETs, other radio-tracers need to be considered and we cannot restrict only to pure β^- decays. There is indeed a significant number of nuclides which have a half-life ($\tau_{1/2}$) compatible with clinical applications and a limited γ radiation. For instance ^{186}Re has $\tau_{1/2} \sim 90$ h and 137 keV photons in only 9% of the cases. To this aim, the design of the detector needs to take into account the existence of a γ radiation, albeit limited, and the softer β^- spectrum (endpoint at 1.1 MeV as opposed to 2.3 MeV).

Finally, the requirements on the detecting probe are driven by the surgical conditions and by the characteristics of the radio-tracers: the probe needs to be sensitive to residuals as small as 0.1 ml, benchmark chosen by the sensitivity of the pre-operative diagnostics; it needs to be directional, i.e. insensitive to radiation from the sides; it needs to have the largest possible detection efficiency on electrons with the smallest sensitivity to photons; the smallest is the minimum electron energy that can be detected, the wider is the applicability of the technique because it allows for more radio-isotopes to be

* Dip. Fisica, Sapienza Univ. di Roma, Rome, Italy; † INFN Sezione di Roma, Rome, Italy; ‡ Center for Life Nano Science@Sapienza, Istituto Italiano di Tecnologia, Rome, Italy. § Dip. Scienze di Base e Applicate per l'Ingegneria, Sapienza Univ. di Roma, Rome, Italy; ¶ Laboratori Nazionali di Frascati dellINFN, Frascati, Italy; ‖ Museo Storico della Fisica e Centro Studi e Ricerche "E. Fermi", Rome, Italy;

used and because it retains the sensitivity to tumor even if a thin layer of other tissues or liquids covers it; finally, it needs to match the security standards for intra-operative use.

In this context, this paper describes the design details of our first prototype and the test in laboratory of its performances. Such tests had to be designed to reproduce by means of phantoms and automated procedures conditions as close as possible to the surgical environment. The outcome of these tests were input to the simulations that were used to estimate the sensitivity of the RGS technique proposed in several clinical cases [8], [9], studies that are preliminary to the clinical tests.

II. The β^- intraoperative probe

In the first prototype of the intraoperative probe (Fig. 1) the radiation sensitive element is a scintillator tip made of commercial poly-crystalline para-terphenyl doped to 0.1% in mass with diphenylbutadiene [10] manufactured by Detec-Europe. This material was adopted, after a detailed study [11], due to its high light yield ($\sim$3 times larger than typical organic scintillators), negligible hygroscopy, and low density, characteristics that minimize the sensitivity to photons. Different detector sizes were tested: the best configuration resulted in a cylinder of 5 mm in diameter and 3 mm in height.

The scintillator tip is shielded from radiation coming from the sides by a black PVC ring with external diameter of 11 mm. A 10 μm-thick aluminium front-end sheet covers the detector window to ensure light tightness. This assembly is mounted on top of an easy-to-handle aluminum cylindrical body (diameter 8 mm and length 14 cm).

In order to avoid the risk of patients coming into contact with electrical devices, the scintillation light is guided by four 50 cm long optical fibres outside the probe to a Hamamatsu H10721-210 photo-multiplier tube (PMT). This photo-sensor module has an integrated high voltage power supply circuit requiring an input voltage as low as 5 V, making this device compatible with the surgical environment. Finally, the read-out electronics and the logic board are housed in a compact box that wirelessly connects to a remote monitor to display the counting rate [12].

III. Characterization of the β^- intraoperative probe

The characterization of the probe response to β^- decays is performed with two ^{90}Sr sources a point-like one with nominal activity of $\sim$370 Bq (*point-source*) and a 1.6 cm diameter source with a 2.54 ± 0.15 kBq activity (*extended-source*). The ^{90}Sr spectrum is made of two components in secular equilibrium: the Sr β^- decay to ^{90}Y and the subsequent β^- decay of the daughter. The latter component is exactly the one relevant for the proposed for RGS if ^{90}Y is used.

A. Efficiency

To reduce the required injected activity it is important to maximize the efficiency. Furthermore, given the fact that even if we are currently considering ^{90}Y as radionuclide different emitters will have to be considered in the future, it is important to know how low in energy the sensitivity of the probe extends. Therefore, we had to setup an ad-hoc measurement to evaluate the efficiency as a function of the emitted electron.

To this aim a vertical scan over the *extended-source* was performed measuring the rate with both the source and the probe in water for several distances (D_w) between the two. The presence of increasing amounts of water dumps the β^- energy spectrum in a way that depends on the energy dependence of the efficiency. On the other hand, the absolute measured rate, and in particular the rate measured at contact (zero water thickness) depends on the absolute efficiency.

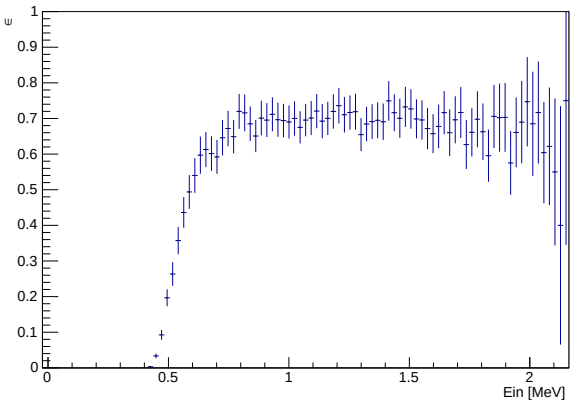

Fig. 3. Probe efficiency as a function of the electron energy (E_{in}).

To correlate the measured rates with the efficiency a Monte Carlo (MC) simulation based on FLUKA code [13] was used. The FLUKA software fully simulates the energy and position spectrum emitted by the source, the energy deposition in water and the probe. It also simulates the light emission and collection with the parameters measured in Ref. [11], returning the number of photoelectrons reaching the PMT (N_{PMT}). The fraction of the electrons that are emitted by the source and reach the detector is estimated by the fraction of the simulated electrons that satisfy the condition $N_{PMT} > N_{thr}$. It has to be stressed that this is not an estimate of the minimum number of photo electrons that are required to have a signal since the quantum-efficiency needs to be taken into account.

The comparison of this estimate with data allowed to extract a value of N_{thr}, in two independent ways. On one side, N_{thr} was tuned to match the measured rate in the configuration where the probe is in contact with the source. The best compatible threshold value was found to be $N_{thr} = 240$. On the other side, N_{thr} affects the dependence of the rate with D_w (see Fig. 2 on the left). A χ^2 of agreement in between the data and MC rate variations between $D_w = 7$ and $D_w = 8.2$ mm was calculated for each value of N_{thr}. Such χ^2 showed a clear minimum in $N_{thr} = 250$ (Fig. 2 on the right).

The two estimates of N_{thr} are compatible and therefore we considered the average $N_{thr} = 245$. To translate this estimate in terms of efficiency as a function of energy, we performed another simulation with the *point-source* and computed the ratio of the electron energy spectrum with and without the requirement $N_{PMT} > N_{thr}$. The result is shown in Fig. 3.

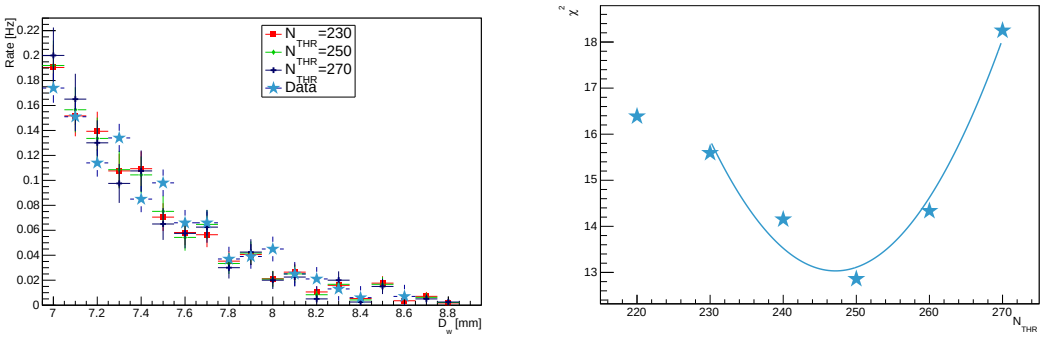

Fig. 2. Left: Dependence of the electron rate as a function of water thickness D_w, in data and in several MC configurations differing by the threshold in the number of photoelectrons. Right: χ^2 of agreement between data and MC (see text) as a function of N_{thr} (N_{thr}).

The efficiency raises at energies above 540 keV (energy at which the curve reaches half of its maximum) and reaches the high energy plateaux at 70%.

B. Spatial resolution

To study the capability of the probe to reconstruct active spots, the detector was mounted on a motorized linear actuator ensuring position accuracy of 1.5 μm and horizontal scans were performed over the *point-source* in air.

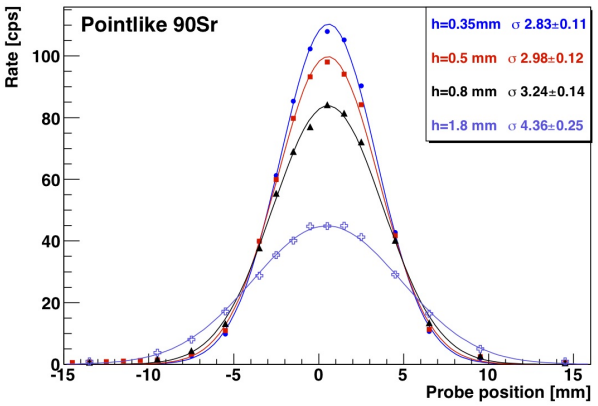

Fig. 4. Profiles of the point-like *Sr-source* reconstructed by the probe at different distances from the source.

An horizontal scan over the point-like *Sr-source* (Fig. 4) allowed to estimate the dependence of the spatial resolution on the distance between the probe tip and the surface. The reconstructed profiles measured at distances ranging from 350 μm to 1.8 mm are fitted using a Gaussian distribution obtaining σ between 2.8 and 4.4 mm.

C. Background rejection capability

The usage of pure β^- emitting tracers allows to operate with low radiation background, the residual being mainly due to photons coming from the *Bremsstrahlung* radiation of the electrons penetrating the tissue. The abundance of the expected *Bremsstrahlung* radiation in the tissue as a function of the photon energy is shown in Fig. 5 as computed with

Figure 1 from Xing Rong et al 2012 Phys. Med. Biol. 57 3711

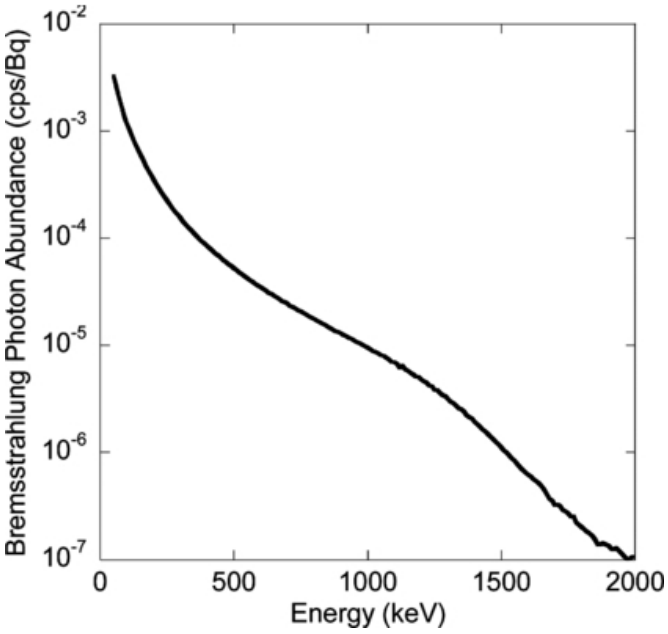

Fig. 5. Energy spectrum (50-2000 keV, 10 keV interval) of ^{90}Y *Bremsstrahlung* photons in water.

a simulation of a ^{90}Y source in water [14]. It is important in any case to ascertain that such radiation does not alter the locality of the measurement. Conversely, in the case non pure β^- emitters are used, it is important to minimize the sensitivity to γs.

To this aim, the sensitivity of the probe to photons was measured using three point-like sources: ^{133}Ba emitting photons with energy ranging from 80 to 350 keV, ^{137}Cs with gamma emission at E_γ=662 keV and ^{60}Co with $E_{\gamma 1}$=1170 keV and $E_{\gamma 2}$=1330 keV. To avoid signal from electrons in the case of Cs decays, three copper layers with 350 μm thickness were inserted in sequence between the source and the probe tip, and the measurements were repeated at each step. The counts as measured by the probe are shown in the Fig. 6 for the three sources. Except for the first measure on the Cs source, introducing the copper absorbers implies a very small decrease in rate compatible with the attenuation in copper and the

change in geometrical acceptance.

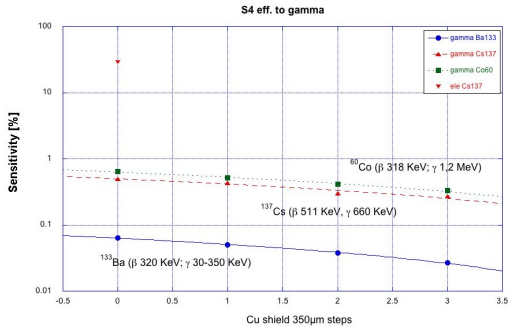

Fig. 6. Probe sensitivity to photons emitted by three different sources: ^{60}Co $E_{\gamma 1}$=1170 keV $E_{\gamma 2}$=1330 keV, ^{137}Cs E_{γ}=662 keV, ^{133}Ba E_{γ} ranging from 80 to 350 keV. The measurements were repeated after insertions of copper layers with thickness of 350 μm between the source and the probe tip to absorb the electronic component of the Caesium emissions.

The sensitivity to the photons emitted by the ^{133}Ba source is 0.06%, whereas for the γs from the ^{137}Cs and ^{60}Co sources the sensitivity is still 0.5%. These measurements allow us to conclude that the intraoperative β^- probe is not sensitive to the *Bremsstrahlung* photons and therefore the effectiveness of the RGS technique would not be affected by this background.

IV. Preclinical tests on specific phantoms

A critical aspect in the test of the prototypes for the development of the new RGS technique, is the difficulty to perform realistic studies before the preclinical test. This aspect is particularly important for this technique because the outcome of the laboratory test is used to evaluate which clinical cases to consider. To this aim, specific phantoms were designed to reproduce finite size meningioma remnants embedded in healthy brain tissue with a TNR as expected in a real clinical case, namely meningioma that is considered the test bench of this technique. The same set-up allows going through different kinds of interfaces and visual/acoustic feedback to identify which one could best assist the surgeon in the search for infected residuals.

A. Realization of the phantoms

The surgical environment is simulated saturating conveniently shaped cuttings of a commercially available sponge (Wettex Classic by Vileda®) with ^{90}Y-DOTATOC in saline solution.

The sponge is made of 65% cellulose and 35% cotton fibres packed as 20×20 cm wide and 2 mm thick dry sheets. The choice of the sponge was driven by its high water absorbency (as measured by us on small samples), the ease of obtaining a sharp and precise cut even with few millimetre wide complex shapes, and the capability of a sample to regain its original dimensions after a wetting-drying cycle.

With this technique, both wet or dry surfaces can be produced depending on the scope of the test: dry phantoms are used to test the neat physics detector performances (e.g. sensitivity to active spots, capability of profile reconstruction); on the contrary, wet surfaces are suitable for studying and optimizing the probe usage in a more realistic environment where, for example, tip contamination might occur adding a random background to the signal coming from the tissues.

The simplest assembly made with this technique is shown in Fig. 7: a 5 mm diameter circular cutting simulating a 0.05 ml tumour residual is inserted inside a larger (20 mm diameter) ring reproducing the nearby healthy tissue. A third round shape (disk) was eventually used to reproduce the presence of further healthy tissues above or under the hot spot. Different TNR between the tumour and the surrounding healthy tissue were realized drenching the cuttings, up to saturation, with the properly diluted ^{90}Y solution. The elements were then dried and combined to shape the topology of interest (Fig. 8).

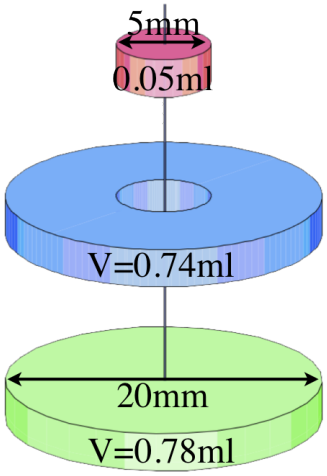

Fig. 7. Assembling of a phantom simulating a **tumour residual** of 0.05 ml embedded in surrounding (the **ring**) and underneath (the **disk**) healthy tissue.

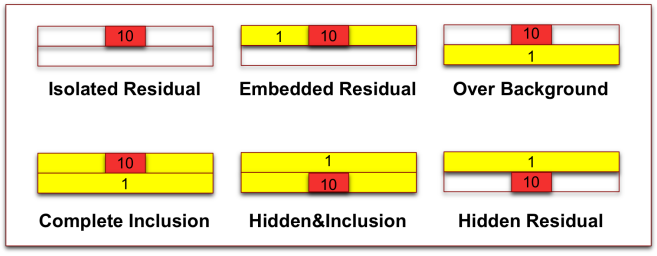

Fig. 8. Varying position and activity (white: non-active tissue, yellow: active tissue) of the assembly elements the discovery potential of the probe can be tested on surfaces reproducing, even if schematically, some possible combinations of cancerous residual location and TNR occurring during surgery.

The nominal activity of any phantom was inferred from the activity of the ^{90}Y-DOTATOC vial at the time of delivery and the dilution factor of the bath prepared to drench the samples. The relative activity of the final dried phantoms was individually measured before forming the assembly.

B. Active spot identification

A scan over the described assembly was performed by fixing the probe to a XZ motorized system. The X linear actuator run

the probe over the phantom in 1 mm steps, with a measurement time of 10 s per position, while the Z actuator was used to set the tip to surface distance with a precision of 1.5 μm.

The different configurations were analyzed in terms of false-positive probability (FP), i.e. the probability that the rate emitted by an healthy tissue is incorrectly flagged by the probe as tumour residual. In the actual case, this flag will be set in real time by the system comparing the signal measured over the tissue under investigation and the patient reference background previously measured over their healthy tissue. The probability of false-positive then depends on the probe efficiency, the time to response and the actual TNR.

An example of a scan is shown in Fig. 9, where the horizontal lines indicate the minimum rate needed to ensure FP$< 1\%$ with a measurement. Below the figure a scheme of the source indicates if the individual regions have the activity associated to background (blue area) or 10 times more (red area). The unfilled area corresponds to non-active regions. The device clearly selects the correct region.

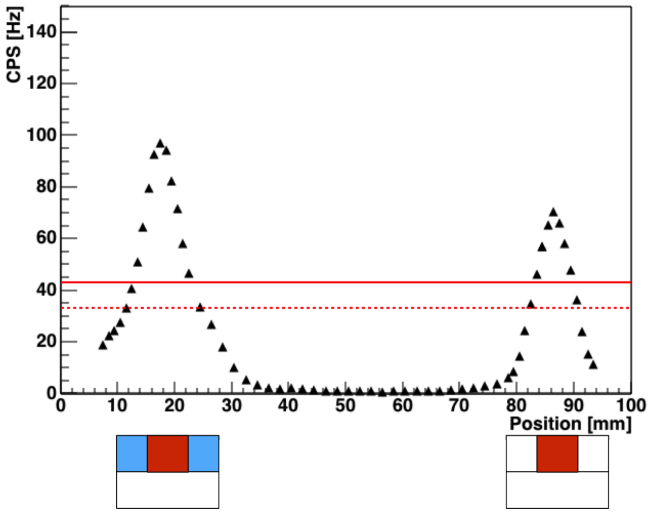

Fig. 9. Scan over two assemblies with a probe tip-surface distance next to zero. The left phantom simulates a 0.5 ml tumour surrounded by a same thickness healthy tissue with a TNR of 10 (as observed in patients affected by meningioma), the second assembly is an isolated residual (non-active surrounding tissue).The full (dashed) line corresponds to the rate needed to ensure a 1% false positive rate in 1 (10) seconds. See the text for details on the source representation below the plot.

Fig. 10 and 11 show the same measurement performed on different tumour-health tissue patterns (fixed the specific activity and the TNR) that might affect the discovery potential of the probe.

These evaluations were performed in a neat and well known configuration, whereas the surgical environment might introduce some perturbations as, for example, a contamination of the probe tip coming into contact with the wet active tissue. Such effect can be evaluated directly from the scan shown in Fig. 9 adding, via software, an extra background to the measure up to the minimum TNR that makes still detectable the hot spot. The study lead to the conclusion that the probe is able to correctly identify the active spot also in case of TNR as low as 2 with $FP = 1\%$ C.L. and a time of measure of 10 s. That means that an eventual contamination would not be

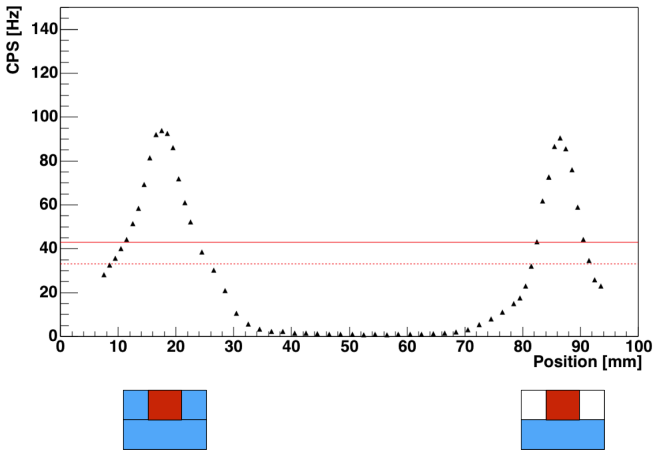

Fig. 10. Scan over two assemblies with a probe tip-surface distance close to zero realized to study the sensitivity of the probe to a 0.5 ml hot spot masked by side and beneath emitting (TNR=10) healthy tissue. The full (dashed) line corresponds to the rate needed to ensure a 1% false positive rate in 1 (10) seconds. See the text for details on the source representation below the plot.

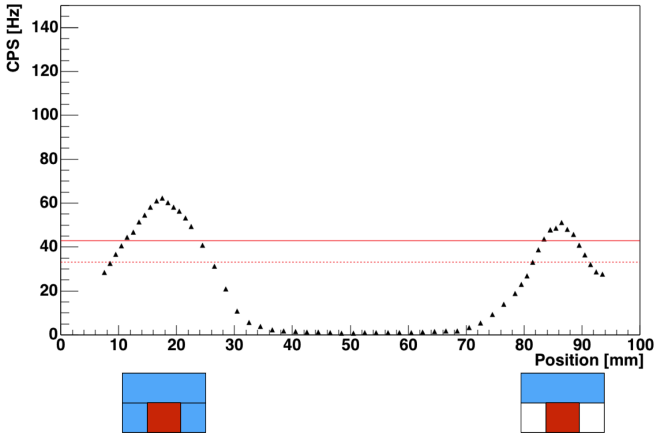

Fig. 11. Scan over two assemblies with a probe tip-surface distance equal to zero to test the sensitivity of the probe to a hot spot hidden under an emitting (TNR=10) healthy tissue. The full (dashed) line corresponds to the rate needed to ensure a 1% false positive rate in 1 (10) seconds. See the text for details on the source representation below the plot.

a problem if monitored with frequent background calibration during the operation.

Moreover, these results imply that the RGS technique with β^- decays would be effective also in case of patients with a lower TNR compared to those affected by meningioma, and therefore they are a confirmation that the RGS could be extended to clinical case of interest with an eventual uptake of the radiotracer in the nearby healthy organs [8].

C. Minimum detectable tumour residual

A different phantom pattern was used to simulate and study the evolution of the probe response while removing an extended tumour area aiming at the identification of the minimum detectable residual. For this purpose the assembly shown in Fig. 12 was used. A scan over the whole strip was repeated reducing the tumoural area by removing a tile at a time starting from the wider one (5 mm). At each iteration the

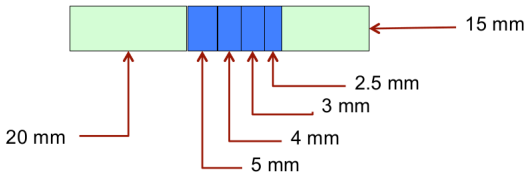

Fig. 12. The phantom prepared to simulate the progress of a surgical removal of a tumour is made by a strip (blue) of 4 tiles of different sizes and charged at the tumour uptake. A sequence of scans was performed removing a strip at each iteration to study the minimum detectable residual. At the beginning and the end of this assembly two tiles (green) ten times less active define the boundary of the healthy tissue surrounding the tumour.

assembly was packed again to always keep the tumour area enclosed between healthy tissues.

The scan over the full 15 mm long tumour phantom is shown in Fig. 13. Following the scan from the right to the left the experimental shape is read as follow: the cps counts start from zero (the probe is outside the scanning area) and increase as the probe goes over the healthy tissue. The small plateau at 30 cps defines the background level of this measure. Approaching the tumour phantom, the counts increase up to plateau at about 250 cps lasting as much as the probe sensitive area is fully illuminated by the tumour area. As soon as the sensitive detector exits the last tumour tile the rate goes back to that of the healthy tissue.

The responses measured reducing the tumour thickness to 3 mm and 2.5 mm are shown in Fig. 14 and Fig. 15 respectively. In both cases the tumour margins are clearly identified once the activity of the surrounding healthy tissue is known.

The smallest residual tested in this measure, obtained reducing by 5 mm the length of the 2.5 mm tile, has a volume of 0.03 ml. The corresponding signal is shown in Fig. 15.

V. Conclusion

We reported on the performances of the first prototype of the intraoperative probe purposely designed to exploit the newly proposed radio-guided surgery with β^- decays. The low density and the high light yield of the para-terphenyl scintillator allow the development of a very compact device with a good sensitivity to electrons in the range of the ^{90}Y decays and almost transparent to the *bremsstrahlung* photons. The first results obtained experimenting the probe on point-like and extended ^{90}Y sources highlight the potentiality of this approach in all the issues relevant in this field: millimetric remnants discovery potential, spatial resolution, fast response, dose administered to the patient, operators safety.

References

[1] Solfaroli Camillocci E, et al., 2014 *Sci. Rep.* **4** 4401
[2] Patent PCT/IT2014/000025 deposited by Università degli studi di Roma "La Sapienza", Istituto Nazionale di Fisica Nucleare and Museo storico della fisica e centro studi e ricerche "E. Fermi".
[3] Povoski SP, et al., 2009 *World Journal of Surgical Oncology* 7-11
[4] Cremonesi M,et al., *J. Nucl. Med.* **47,** 1467-1475 (2006); Cremonesi M, et al. *Q. J. Nucl. Med. Mol. Imaging* **54,** 37-51 (2010)
[5] Heppeler A, et al., 1999 *Chem Eur J* **7** 1974-81
[6] Bartolomei M, et al., 2009 *Eur J Nucl Med Mol Imaging* **36** 1407-16

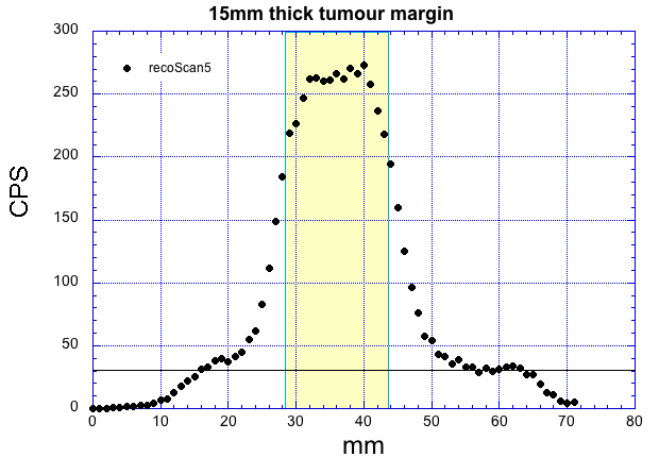

Fig. 13. A scan over a 15×10 mm^2 tumour activated phantom. The yellow area indicate the position of the tiles between the two healthy tissue phantoms. The limited lateral shield makes the probe sensitive to the approaching active area about 4 mm before the detector goes over the hot tiles.

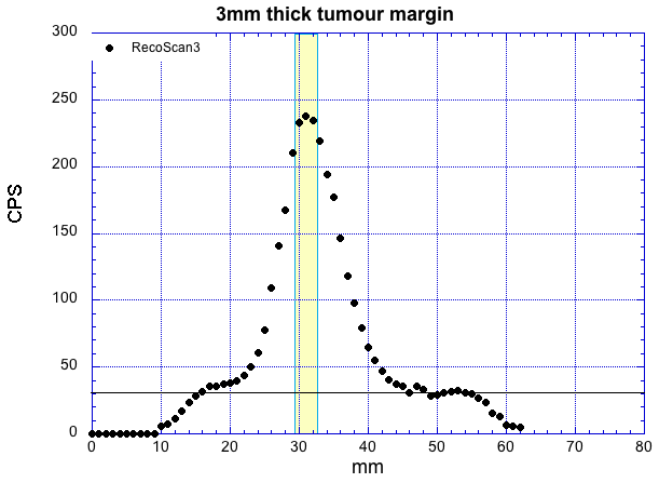

Fig. 14. Scan over a 3 mm wide tumour tile phantom. Since the width of the phantom is smaller than the sensitive detector dimension, the distribution shows a peak corresponding to the alignment centred over the sample.

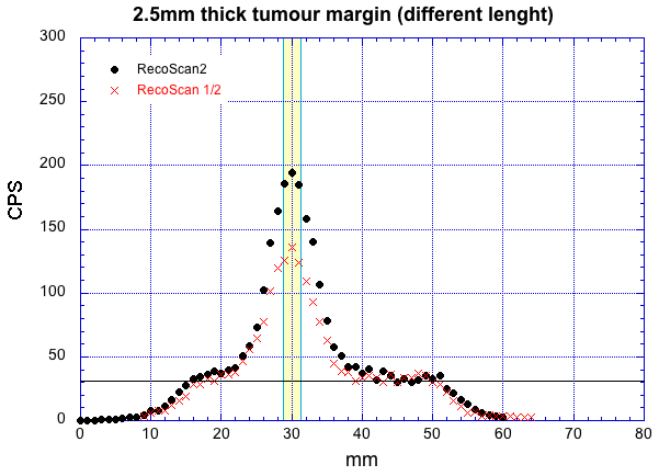

Fig. 15. Scan over a 2.5×10 mm^2 tumour margin. The red cross refers to the same scan performed on a smaller 2.5×5 mm^2 sample.

[7] Kunikowska J, et al., *E*ur J Nucl Med. 2011; 38: 1788-97.
[8] Collamati F, et al., 2015 *J Nucl Med* **56** 1-6
[9] Collamati F, et al., 2015 "Time evolution of DOTATOC uptake in Neuroendocrine Tumors in view of a possible application of Radio-guided Surgery with β^- Decays." Submitted to *J Nucl Med*
[10] Budakovsky SV, et al., 2009 *Functional Materials* **16**, 1 86-91
[11] Angelone M, et al., 2014 *IEEE Transactions on Nuclear Science* **61**, 3 1483-87
[12] Bocci V, et al., arXiv:1411.7814v1
[13] Ferrari A, et al., 2005 *Tech. Rep.* CERN-2005-10, INFN/TC05/11, SLAC-R-773
[14] Rong X, et al., 2012 *Phys Med Biol* **57** 3711-25